

# An H-Adaptive Finite Element Method for Turbulent Heat Transfer

David B. Carrington<sup>1</sup>, Xiuling Wang<sup>2</sup> and Darrell W. Pepper<sup>3</sup>

**Abstract:** A two-equation turbulence closure model ( $k$ - $\omega$ ) using an h-adaptive grid technique and finite element method (FEM) has been developed to simulate low Mach flow and heat transfer. These flows are applicable to many flows in engineering and environmental sciences. Of particular interest in the engineering modeling areas are: combustion, solidification, and heat exchanger design. Flows for indoor air quality modeling and atmospheric pollution transport are typical types of environmental flows modeled with this method. The numerical method is based on a hybrid finite element model using an equal-order projection process. The model includes thermal and species transport, localized mesh refinement (h-adaptive) and Petrov-Galerkin weighting for stabilizing advection.

This work develops the continuum model of a two-equation turbulence closure method. The fractional step solution method is stated along with the h-adaptive grid method (Carrington and Pepper, 2002). Solutions are presented for 2d flow over a backward-facing step.

## 1 Introduction

Understanding turbulent flow for problems has been of interest for over a century, dating back to Boussinesq when he introduced the idea of an eddy viscosity in addition to molecular viscosity, and to Reynolds who developed what is now called Reynolds time averaging. Various ideas have been developed to achieve a closure to the momentum equations, that is, to determine ways to solve the Reynolds stress terms. In 1942 Kolmogorov developed the  $k$ - $\omega$  which provides the turbulent length scale,  $k^{1/2}/\omega$  where  $1/\omega$  is the turbulent time scale. The two-equation model is a complete model because it does not require a priori knowledge of the turbulent flow to solve the equations.

---

<sup>1</sup> Los Alamos National Laboratory, T-3, Los Alamos, NM

<sup>2</sup> Purdue University, Calumet, IW

<sup>3</sup> University of Nevada, Las Vegas, NV

Many methods have been developed to model turbulence and solve the turbulent momentum system. In the time-averaging genre are models ranging from simple zero and one-equation models, various forms of the two-equation model. Wang, Carrington and Pepper (2009) implement a low-Re  $k-\epsilon$  model in an adaptive FEM method demonstrating the accuracy of the results over the backward-facing step. Naj and Mompean (2009) demonstrate a cubic low-Re  $k-\epsilon$  model in a Finite Volume (FV) formulation (and compare that to Direct Numerical Simulation (DNS) for flow in a square duct.

As with the models, various methods exist for the discretization, e.g., the FEM described in this paper, the FV and Meshless techniques as developed by Lin and Atluri (2000) via a Moving Least Square (MLS). Vertnik and Sarler (2009) employ meshless method using radial basis functions for solving  $k-\epsilon$  closure model with the pressure projection method as described in this paper for momentum solution.

In this paper a  $k-\omega$  model two-equation closure method is employed in a grid adaptive (refinement) Finite Element Method (FEM). Many aspects of the  $k-\omega$  model make it attractive. For example, the 2 equations, turbulent kinetic energy ( $k$ ) and specific dissipation rate ( $\omega$ ), can be integrated to a solid wall. The usual system employs wall functions based on the wall laws. Also, the model has nice properties at low Reynolds number; it works well through the unsteady transition regimes and behaves better than the  $k-\epsilon$  model in flow with recirculation and those flows with adverse pressure gradients (Wilcox, 2003).

In particular, the  $k-\omega$  model and its implementation are examined with solutions for 2d flow. The solution method for the Reynolds averaged equations is performed by the fractional step method (Carrington and Pepper, 2002). Also, the method employs a Petrov-Galerkin (P-G) upwinding scheme (Kelly, et al., 1980; Heinrich and Yu, 1988). This is the same type of scheme as applied by Lin and Atluri in their work with Moving Least Square and local Petrov-Galerkin meshless methods (2000).

## **2 Physical model**

Fluids are governed by mass conservation (continuity) and the conservation of momentum and energy. By averaging these equations in time (Reynolds time averaging) the instantaneous equations result in additional terms, the Reynolds stresses or turbulent stresses.

Turbulent flows are characterized by eddies with a wide range of length and time scales. The largest eddies are typically comparable in size to the characteristic length of the mean flow. The smallest scales are responsible for the dissipation of turbulence kinetic energy. Creating time average Navier-Stokes equations by

Reynolds averaging (Tennekes and Lumley, 1972) one obtains:

$$\frac{\partial \rho}{\partial t} + \frac{\partial (\rho \bar{u}_i)}{\partial x_i} = 0 \quad (1)$$

$$\frac{\partial (\rho \bar{u}_i)}{\partial t} + \frac{\partial (\rho \bar{u}_i \bar{u}_j)}{\partial x_j} = \frac{\partial}{\partial x_j} \left( \mu \frac{\partial s_{ij}}{\partial x_j} \right) - \frac{\partial \bar{p}}{\partial x_j} - \frac{\partial \tau_{ij}}{\partial x_j}. \quad (2)$$

In familiar incompressible form the momentum equation is

$$\rho \frac{\partial \bar{u}_i}{\partial t} + \rho \bar{u}_j \frac{\partial \bar{u}_i}{\partial x_j} = - \frac{\partial P}{\partial x_i} + \frac{\partial}{\partial x_j} \left( \mu s_{ij} - \overline{\rho u'_i u'_j} \right) \quad (3)$$

where  $s_{ij}$  is the strain rate tensor due to molecular viscosity, and  $\tau_{ij}$  is the Reynolds stress tensor given by

$$\tau_{ij} \equiv \overline{\rho u'_i u'_j} \quad (4)$$

The momentum equation has 6 new unknowns related to the Reynolds stress tensor, for a total of 10 unknowns in 3 dimensional flows. Transport equations for the Reynolds stress tensor are derived from a moment of the momentum equation for fluctuations. Modeling the equations directly is Reynolds stress modeling. The derivation is lengthy, and is well presented in many texts, e.g., Wilcox's "Turbulence Modeling for CFD" (2003). These six unknowns in the Reynolds stress tensor create a closure problem which can be modeled with higher moments, e.g., a two-equation model with closure coefficients. The system is not fully closed without some form of analysis to determine the closure coefficients.

Simplifying the equation, that is, creating a model that is less complicated and gives an estimate to the Reynolds stress can be performed using the average velocity terms. The Reynolds stresses can be made of the form

$$\tau_{ij} = \mu_t \left( \frac{\partial \bar{u}_i}{\partial x_j} + \frac{\partial \bar{u}_j}{\partial x_i} \right) - \frac{2}{3} \delta_{ijk} k, \quad (5)$$

by introducing a turbulent viscosity,  $\mu_t = \rho c_u k^2 / \varepsilon$  and  $\varepsilon$  is the turbulent dissipation rate. Turbulent kinetic energy is transported having both generation and dissipation terms.

Turbulent kinetic energy, when using the Boussinesq assumption, is given by

$$\rho \frac{\partial \vec{k}}{\partial t} + \rho (\vec{u} \cdot \nabla) \vec{k} = c_2 \mu_t \nabla^2 \vec{k} + \vec{P}_k - \nabla \vec{D}_k - \vec{\varepsilon}. \quad (6)$$

where we now assume all velocities are averaged, except where noted, and where  $c_2$  is a closure coefficient. Turbulent production  $P_k$  is given by,

$$P_k = \tau_{ij} \frac{\partial u_i}{\partial x_j} = \left[ \mu_t \left( \frac{\partial u_i}{\partial x_j} + \frac{\partial u_j}{\partial x_i} - \frac{2}{3} \frac{\partial u_k}{\partial x_k} \delta_{ij} \right) - \delta_{ij} \frac{2}{3} \rho k \right] \frac{\partial u_i}{\partial x_j} \quad (7)$$

the turbulent diffusion  $D_k$  is

$$D_k = - \frac{\rho \mu_t}{\sigma_k} \frac{\partial k}{\partial x_j}, \quad (8)$$

and turbulent dissipation rate  $\varepsilon$ , (noting the averaged fluctuating components) is

$$\varepsilon = \mu \frac{\partial u'_i}{\partial x_j} \frac{\partial u'_i}{\partial x_j}$$

The units for turbulent kinetic energy is  $\text{length}^2/\text{time}^2$  and  $\varepsilon$  has units of  $\text{length}^2/\text{time}^3$ .

## 2.1 Two-Equation Closure Model

The  $k$ - $\omega$  two-equation model incorporates an effective viscosity formulation for the Navier-Stokes equation, stated as

$$\frac{\partial (\rho u_i)}{\partial t} + \frac{\partial (\rho u_i u_j)}{\partial x_j} = \frac{\partial}{\partial x_i} \left( (\mu + \mu_t) \left( \frac{\partial u_i}{\partial x_j} + \frac{\partial u_j}{\partial x_i} \right) \right) - \frac{\partial p}{\partial x_j} \quad (9)$$

where

$$\mu_t = \bar{\rho} k / \omega. \quad (10)$$

Specific dissipation rate and dissipation rate are related by

$$\varepsilon = \beta^* \omega k, \quad (11)$$

and the mixing length is

$$l = k^{1/2} / \bar{\omega}. \quad (12)$$

Turbulent kinetic energy (as above with the addition of closure coefficient for  $k$ ), and dissipation rate  $\omega$  are, respectively,

$$\rho \frac{\partial k}{\partial t} + \rho u_j \frac{\partial k}{\partial x_j} = \frac{\partial}{\partial x_i} \left[ (\mu + \sigma^* \mu_t) \frac{\partial k}{\partial x_j} \right] + P_k - \beta^* \rho k \omega \quad (13)$$

$$\rho \frac{\partial \omega}{\partial t} + \rho u_j \frac{\partial k}{\partial x_j} = \frac{\partial}{\partial x_i} \left[ (\mu + \sigma \mu_\tau) \frac{\partial \omega}{\partial x_j} \right] + \alpha \frac{\omega}{k} P_k - \beta \rho \omega^2 \quad (14)$$

These types of moment equations require closure coefficients because succeeding higher order moments are always neglected, ad infinitum. Turbulent modeling requires closure coefficients. It is an open ended problem in continuum formulation, discretization at longer than the Kolmogorov scale. For the  $k$ - $\omega$  Eq. 14 and 15, these coefficients are:

$$\begin{aligned} \alpha &= 5/9, & \beta &= 3/40, & \beta^* &= 9/100, \\ \sigma &= 1/2, & \sigma^* &= 1/2, & \mu_\tau &= \rho k / \omega \end{aligned} \quad (15)$$

The specific dissipation rate is a measure of the root mean square of the fluctuating vorticity with units of inverse time, 1/time.

### 3 Finite Element Model

To apply the finite element method to the solution of the governing equations the weak statements of the equations are found and then coded. The energy and mass transport equations are included below in the development. These will be needed to solve convective and species transport problems. The Method of Weighted Residuals is applied to the weak statements resulting in the following representation of the governing equations. Note that the vectors are trial functions as is the turbulent viscosity and turbulent heat dispersion, i.e.,

$$Z_i = \sum_{n=1}^N \varphi_n(x) z_i^n(t) = [N_j] \{Z_i\}, \quad (16)$$

where  $Z_i$  is any dependent variable,  $[N_j]$  is the basis (shape) function notation for the element  $\square$  is a row vector (row matrix), the transpose of a column vector  $\{\}$ . Other terms in the following weak statements include the integral over the domain or element  $\int_{\Omega} d\Omega$  and over the boundary surface  $\int_{\Gamma} d\Gamma$ . The specifics of evaluating the boundary term is presented after combining the following into matrix equations, where the boundary terms become the load vector in the matrix statement.

#### 3.1 Matrix equations

By integrating each element and combining the contributions from each element to nodes in common to those elements, a matrix equation is formed that will be solved for the nodal values. The specific components of these matrix equations are described by Carrington and Pepper (2002), Carrington (2002); Pepper and Carrington (2009).

The matrix equations for the explicit time advancement of momentum, heat and mass transport can be written as

$$[\mathbf{M}] \{\dot{\mathbf{V}}\} + [\mathbf{A}(\mathbf{V})] \{\mathbf{V}\} - \mathbf{C}\{\mathbf{P}\} + [\mathbf{K}_v] \{\mathbf{V}\} = \{\mathbf{F}_v\} \quad (17)$$

$$[\mathbf{M}_T] \{\dot{\mathbf{T}}\} + [\mathbf{A}(\mathbf{V})] \{T\} + [\mathbf{K}_T] \{T\} = \{\mathbf{F}_T\}, \quad (18)$$

$$[\mathbf{M}] \{\dot{k}\} + [\mathbf{A}(\mathbf{V})] \{k\} + [\mathbf{K}_k] \{k\} = \{\mathbf{P}_k\} + \{\beta^* \mathbf{k}\mathbf{w}\} + \{\mathbf{F}_k\} \quad (19)$$

$$[\mathbf{M}] \{\dot{\omega}\} + [\mathbf{A}(\mathbf{V})] \{\omega\} + [\mathbf{K}_\omega] \{\omega\} = \{\alpha \mathbf{k}/\omega\} \{\mathbf{P}_k\} + \{\beta \mathbf{w}^2\} \{\mathbf{F}_\omega\} \quad (20)$$

### 3.1.1 Time advancement of the Explicit and Implicit Matrix Equations

The initial guess of velocity is marched in time explicitly by

$$\{\mathbf{V}_i^{n+1}\} = \{\mathbf{V}_i^n\} + \Delta t [\mathbf{M}^{-1}] [\{\mathbf{F}_{v_i}\} - [\mathbf{K}_v] \{\mathbf{V}_i^n\} - [\mathbf{A}(V)] \{\mathbf{V}_i^n\} + [\mathbf{C}] \{\mathbf{P}_i^n\}]. \quad (21)$$

This explicit marching applies equally to the scalar quantities of temperature, turbulent kinetic energy, specific dissipation rate, and species transport. Before marching these quantities forward in time, the velocities need to be projected onto the divergence free field.

### 3.1.2 Velocities

The velocities are updated from the components of P

$$\mathbf{V}^{n+1} = \mathbf{V}^* + dt \mathbf{M}^{-1} \mathbf{C} \mathbf{P}. \quad (22)$$

### 3.1.3 Pressure

The pressure is calculated from either the discretized Poisson equation or is extracted directly from the projection algorithm by dividing  $\lambda$  with  $dt$ . This pressure is associated with the projection, the time advanced divergent velocity and is an Euler-Lagrange variational subject to the mass conservation constraint. To calculate the dynamic pressure experienced in the momentum equations, the gradient is taken of the divergent free Navier-Stokes equations, resulting in the Poisson equation. A better estimate of the pseudo-velocity is given by using the dynamic pressure in the velocity predictor.

### 3.1.4 Energy and Species Concentration

Scalar transport for enthalpy (or internal energy) and species is performed as per the scalar transport equation

$$\{\mathbf{T}_i^{n+1}\} = \{\mathbf{T}_i^n\} + \Delta t [\mathbf{M}^{-1}] [\{\mathbf{F}_{v_i}\} - [\mathbf{K}_T] \{\mathbf{T}_i^n\} - [\mathbf{A}(\mathbf{V})] \{\mathbf{T}_i^n\}] \quad (23)$$

Time-step size should be a consideration on this explicit statement. The time scale of most engineering and environmental problems is governed by the faster time scales of turbulence and momentum transport.

### 3.1.5 Turbulent Kinetic Energy and Specific Dissipation Rate

Scalar transport for turbulent kinetic energy and species is performed as a scalar transport

$$\{K_i^{n+1}\} = \{K_i^n\} + \Delta t [\mathbf{M}^{-1}] \left[ \begin{array}{l} \{\mathbf{F}_k\} + \{\mathbf{P}_k\} + \{\beta^* \mathbf{k} \mathbf{w}\} - \\ [\mathbf{K}_k] \{K^n\} - [\mathbf{A}(\mathbf{V})] \{K^n\} \end{array} \right] \quad (24)$$

$$[\mathbf{M}] \{\bar{\omega}\} = \{\omega_i^n\} + \Delta t [\mathbf{M}^{-1}] \left[ \begin{array}{l} \{\mathbf{F}_{\bar{\omega}}\} + \{\alpha \mathbf{k} / \bar{\omega}\} \{\mathbf{P}_k\} + \{\beta \mathbf{w}^2\} - \\ [\mathbf{K}_{\bar{\omega}}] \{\omega\} - [\mathbf{A}(\mathbf{V})] \{\bar{\omega}\} \end{array} \right] \quad (25)$$

where the specific components of these matrix equations are found described by Pepper and Carrington (2009).

The explicit and implicit equations for velocity and pressure are always solved to the boundaries, based on the latest update to the boundary conditions, i.e., those boundaries which are changing with the flow. These are the turbulent closure model boundary conditions  $k$ ,  $\bar{\omega}$  and  $\mu_t$ , which are discussed next along with boundaries for velocity, energy and pressure. When using the law of the wall, the  $k - \bar{\omega}$  equations are only solved to the point next to the solid boundary because the boundary for these points is determined by the wall function. Otherwise the model can be solved to all boundaries provided the grid resolution is sufficient enough to provide for accurate solution in the boundary layer.

### 3.1.6 Boundary Conditions

Dirichlet boundary conditions for average velocity are straightforward: either a no-slip condition for solid objects or fixed velocity at inlets is specified. Outlet boundary conditions can be made with the assumption of a zero gradient for velocity, a Neumann condition. The zero gradient assumption on velocity at outflow requires the computational domain or grid to be constructed to match this imposed boundary condition. This statement can be relaxed with the use of the viscous boundary condition as described by Gresho (1985). Details of the momentum boundary conditions are given by Carrington and Pepper (2002)

### 3.1.7 Wall Law

The solution to the wall condition progresses by iteration since it is transcendental relation. Wilcox (2003), demonstrates the appropriate equation to solve at a

distance ‘ $y_p$ ’ from the wall in the presence of an adverse pressure gradient is

$$u_p = u^* \left[ \frac{1}{k_{vk}} \ln \left( \frac{\rho u^* y_p}{\mu} \right) + B - 1.13 \frac{y_p}{\rho (u^*)^2} \frac{dP}{dx} \right], \quad (26)$$

where  $u_p$  is the tangential velocity at that grid point  $p$ ,  $B$  is a surface roughness factor, and  $k_{vk} = 0.41$ , is the von Karman constant. The equations for turbulent kinetic energy,  $k$  and  $\omega$  in the inner layer are

$$k_p = \frac{(u^*)^2}{\sqrt{\beta^*}} \left[ 1 + 1.16 \frac{\rho u^* y_p}{\mu} P^+ \right], \quad (27)$$

$$\omega_p = \frac{u^*}{k_{vk} y \sqrt{\beta^*}} \left[ 1 - 0.30 \frac{\rho u^* y_p}{\mu} P^+ \right]. \quad (28)$$

Surface roughness can be determined in terms of sand grain size as found experimentally by Nikuradse (Schlichting, 1979).

The wall law for thermal flux where temperature is specified can be given by

$$q_w = (T_w - T_p) \rho c_p k^{1/2} \beta^{1/4} / T^+. \quad (29)$$

where  $T^+$  is described in Lacasse, et al. (2004). In this study, we integrate the domain to the boundary using the wall law only for the turbulence model. This compares to the experimental data, and a restricted computational domain is not used for Neumann conditions.

#### 4 Grid Refinement

The use of  $h$ -adaptation yields accurate solutions and a steeper convergence rate, with error determined by the well established bound or standard error estimate

$$\|u - u_h\|_m \leq ch^{k+1-m} \|u\|_r, \quad (30)$$

where the true solution ‘ $u$ ’ is assumed smooth in the  $H^{k+1}$  Sobolev norm, ‘ $u_h$ ’ the approximate,  $h$  the mesh parameter,  $k$  degree of interpolate (element shape function),  $m$  is chosen norm space, and  $r = k + 1$ , the degree of square integrable derivatives in  $H$  (Hughes, 2000).

The use of  $h$ -adaptive methods has been shown to be effective in modeling environmental transport problems (Pepper and Carrington, 1999). This is particularly important when encountering singularities at (problem geometry) corners, eliminating the need for a graded mesh. Adaptive grid techniques are a common practice.

Recently Peter Lucas, et al. (2009) developed a k- $\epsilon$  model for investigating flow around wind turbines using h-adaptive grid techniques on hexahedral grids, similar to what is discussed and developed in this research.

Adjustments to a discretized domain are designed to increase the resolution and accuracy of solutions to partial differential equations. Discussed in this section is one form of h-type mesh enrichment and its implementation. The idea of using self-adaptive grids has been pursued since around 1970, when it was apparent that to solve large-scale problems practically one should use an optimal grid. Numerous researchers have been developing methods for adaptation and determining how the adaptation process is to be controlled to find an optimal grid (Babuska, 1976; Demkowicz, et al, 1989; Zienkiewicz O.C., 1989).

The goal of adaptation is to achieve the proper mesh, one that significantly improves the computational speed, resolution, and reduces error.

#### 4.1 Mesh Augmentation

Embedding elements within the existing grid is h-adaptation. It is a straight forward procedure that is quickly processed. This is commonly called mesh enrichment. Mesh enrichment can take place in a number of ways. In this work, division of a single element is performed. When hanging or virtual nodes exist (nodes that are not vertices of adjacent elements), the interface zones require special treatment because flux must balance. This is accomplished either by using a nodal constraint (producing a non-positive definite system of equations) or by using an adjusted shape function for the adjoining (coarse) element.

#### 4.2 Implementing Adaptation

There are many error estimators that can be used as the basis for adaptation, e.g., the element-residual method, interpolation methods, subdomain-residual methods, and projection method. Detailed descriptions of these estimators of error can be found in: Ainsworth and Oden (2000), Demkowicz, et al. (1989), Zienkiewicz, O. C. and R. J. Z. Zhu (1987).

The simple residual error estimator as described by Ainsworth and Oden (2000) was used in this study. These errors can be expressed in certain norms such as the “Energy” norm or “ $L_2$ ” norm. The corresponding “ $L_2$ ” residual error, where  $e$  is residual of the most recently solved value, can be written as

$$\|e_\sigma\| = \left( \int_{\Omega} e_\sigma^T e_\sigma d\Omega \right)^{1/2}, \quad (31)$$

where all element errors are typically defined as

$$\|e_\sigma\|^2 = \sum_{i=1}^m \|e_\sigma\|_i^2, \quad (32)$$

where  $m$  stands for the total number of elements. We can now define the error indices  $\eta = \eta_\sigma$  in the form of error percentage as:

$$\eta_\sigma = \left( \frac{\|e_\sigma\|^2}{\|\sigma^*\|^2 + \|e_\sigma\|^2} \right)^{1/2}. \quad (33)$$

The error index  $\eta$  is used to guide the adaptation procedure. In real cases, the decision in choosing which one or combination of variables as the key adaptation variables depends on the problem and its physics.

## 5 Benchmark Solution

Algorithms and computer codes are verified and then validated with experimental data. When numerical solutions of benchmark problems having already been established these solutions also can be used for validating new algorithms and software. Verification involves the process of understanding the model equations and their implementation. Verification answers the question of, “Are the model equations represented correctly.” Validating a particular implementation is the process of determining whether the model equations and their numerical representation are capable of solving the modeled phenomena correctly.

Here we present solutions to a problem that will gauge the accuracy of the model’s implementation: flow over the a 2-D backward-facing step. Flow and heat transfer over a backward facing step (Fig. 1) are more challenging. This problem is of interest to researchers in the areas of combustion, solidification, environmental flow and compact heat exchanger design, etc. Study of flow and heat transfer over a backward-facing step has been a good benchmark problem because of its simplistic geometry, richness of flow physics, and availability of experimental data. Interesting physical phenomena include unsteady behavior, separation, recirculation, reattachment, and a three-dimensionality of the flow. Some who have investigated using particle Velocimetry are Schram, et al. (2004) and Kostas, et al. (2002). Bassem Armaly, et al. (1983) provided both experimental and theoretical investigation to the backward-racing step flow in the laminar flow regime. Gartling (1990) proposed using the backward facing step geometry as a test-problem for outflow boundary conditions. Vogel & Eaton’s experiments (1985) provide experimental data for convective turbulent flow over a backward facing step with an expansion-ratio of 1.25, or 4 step heights to 1.

Depending on the Reynolds number, various recirculation zones set up at the center plane as shown in Fig. 1.

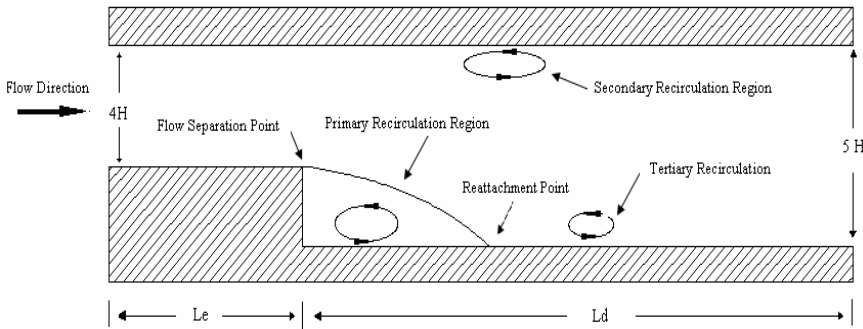


Figure 1: Schematic of the Two-Dimensional Backward-Facing Step showing recirculation areas for unsteady flow.

At low Reynolds numbers ( $Re$ ) flow is laminar and steady. When  $Re$  increases, a recirculation zone downstream of the back step forms and flow becomes unsteady. The loci of reattachment points (reattachment line) are known to oscillate back and forth. In transition regime in addition to the primary recirculation pocket downstream of the back step, two additional recirculation pockets are formed. One is on the top of the duct and one is downstream of the primary recirculation pocket as shown in Fig. 1. As  $Re$  increases further these two additional recirculation pockets disappear and flow becomes turbulent.

Investigating flow over the 2-D backward-facing step using a  $k-\omega$  two-equation turbulent closure modeled by FEM and using an h-adaptive grid demonstrates that the model appears to be well suited for the transition to turbulent regimes. The solution method incorporates uncoupled enthalpy transport. Eventually chemical reactions and radiation phenomena will be added to the model.

The physics of flow over backward-facing step in the laminar, transitional and low Reynolds number turbulent regimes was studied experimentally by Armaly et al. (1983).

The 2-D backward-facing step is merely a tool for benchmarking. It assumes flow in very a wide duct to achieve two-dimensionality that somehow the flow symmetrically along the center plane. This assumption is not precisely accurate. Therefore, investigators have been developing solutions to flow over a 3-D backward-facing

step, where the symmetry assumptions may not be applicable in the unsteady and higher-flow regimes.

Williams and Baker (1997) performed numerical investigations of laminar flows over a three-dimensional backward-facing step. They employed the continuity constraint method (CCM) in conjunction with the Galerkin finite element technique to solve the unsteady three-dimensional Navier-Stokes equations. An implicit scheme was used to march in time. They found agreement of their results with the experimental data of Armaly et al. (1983).

Pepper and Carrington (1997) introduced forced convective heat transfer using a finite element method and the pressure-projection method for this problem. They have reported good agreement of their results with the experimental data in the low transition regime at  $Re = 800$  (Carrington and Pepper, 2002).

Chiang and Sheu (1999) also simulated the three-dimensional laminar flow over a backward-facing step. Euler implicit scheme was used for the time derivatives. Good agreement with the experimental data was found.

### 5.1 Flow Over 2-D Backward-Facing Step

Solutions for flow over a 2-D backward-facing step are presented in Figs. 2 through 7. The flow  $Re=28,000$ , scaled by the step height. The  $Re$  is determined by a density of  $1.1774 \text{ kg/m}^3$ , an inlet velocity of  $17.5 \text{ m/sec.}$ , a dynamic viscosity  $\mu=1.846 \times 10^{-5} \text{ (N sec/m}^2\text{)}$ , and a step height of  $1/5^{th}$  the overall height, or a hydraulic diameter of  $0.025 \text{ meters}$ . The outlet is  $0.15 \text{ meters}$  high, and inlet of  $0.1 \text{ meters}$ . The inlet turbulent kinetic energy is  $k=0.28$  and specific dissipation rate at the inlet is  $\omega = 770$ , resulting in an inlet turbulent viscosity of  $3.7 \times 10^{-3}$ . The grid consists of  $11128 \text{ elements}$ , and  $11385 \text{ nodes}$ . The inlet turbulent  $Re_t$  number is determined by

$$Re_t = \frac{\rho k}{\omega \nu} = \frac{1.1774 \times 0.28}{770 \times 1.846 \times 10^{-5}} = 24.$$

The lower wall downstream of the step has a heat flux,  $q_{wall}$  applied equal to  $270 \text{ (W/m}^2\text{)}$ . The final grid consists of  $62,846 \text{ elements}$ , and  $64,169 \text{ nodes}$  at two levels of enrichment. The initial grid was enriched to one level nearly everywhere except near the outflow and inlet away from the boundary layer. The second level of enrichment is seen in Fig. 2, with more enrichment in the boundary layer and around the expansion.

The state of the flow is shown in the figures at hydrodynamic steady state as determined by the L2 norm of the dependent variables to be less than  $1e-06$ . The thermal properties are: a conductance of  $\kappa=0.02624 \text{ (W/m-K}^o\text{)}$ , a specific heat at constant pressure  $c_p=1.057 \times 10^3 \text{ (J/kg-K}^o\text{)}$  and a turbulent Prandtl number  $Pr_t=0.899$ .

Figure 3 shows the velocity vectors, at every 5<sup>th</sup> node point (and 2 levels of adaptation). The results compare favorably to Vogel and Eaton's results (1985) also to others' (Nallasamy, 1987). In particular, the recirculation length, or region matches experimental results, at 6.4 h, where h is the step height. This length is the standard gauge of the benchmark.

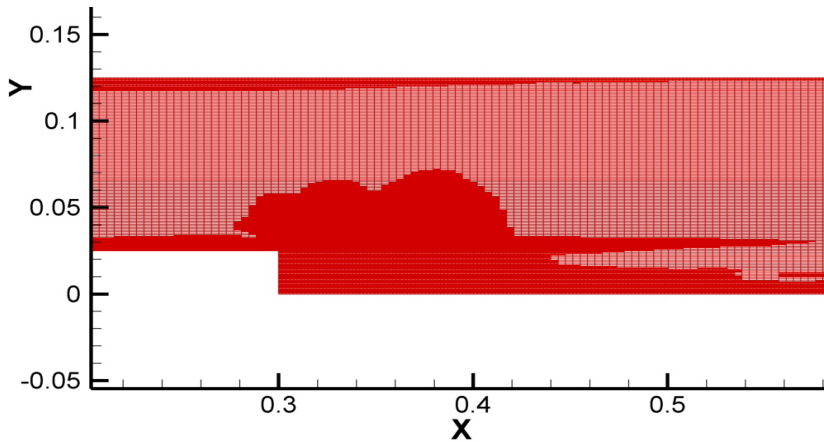


Figure 2: Two levels of enrichment for final adapted grid.

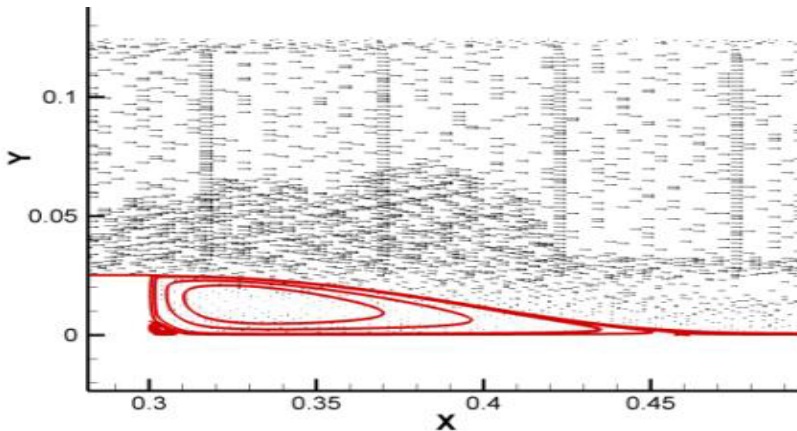


Figure 3: Vectors on refined grid for flow over a 2-D backward-facing step at  $Re=28,000$

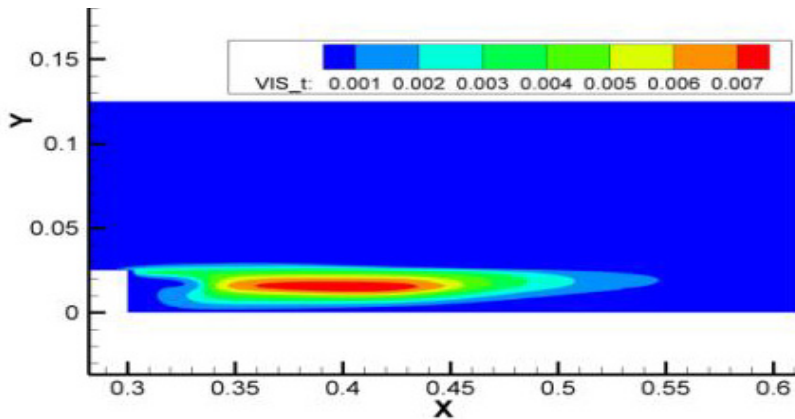


Figure 4: Effective viscosity distribution behind step.

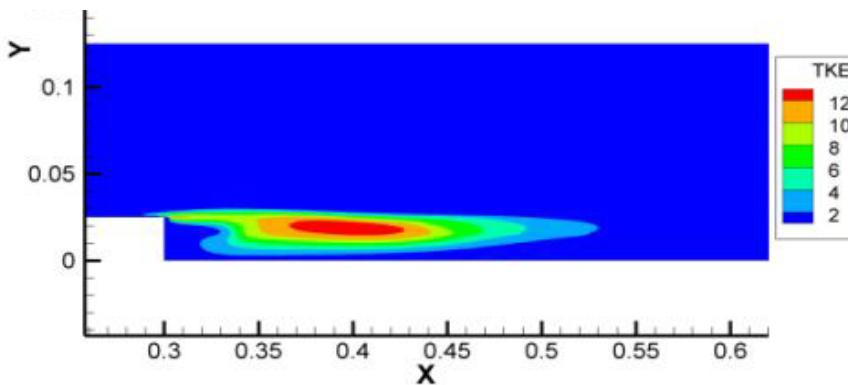


Figure 5: Turbulent kinetic energy distribution behind step.

Figures 4, 5 depict the effective velocity and turbulent kinetic energy behind the step, respectively. The contours are in general agreement with other results (Pelletier et al., 1994; Ilinca, et al., 1998).

Normalized velocity profiles are shown in Fig. 6 as a function of recirculation length where  $U_o$ , is the inlet velocity. A comparison is shown to results from Vogel and Eaton. The distance behind the step is shown as a function of  $x^* = (x-x_r)/x_r$ . The results for the turbulent closure equations and the velocity field are in reasonable agreement with the experimental data. There is some error in the charts associated with digitizing the experimental data from the hard copy journal paper, particularly near the wall region.

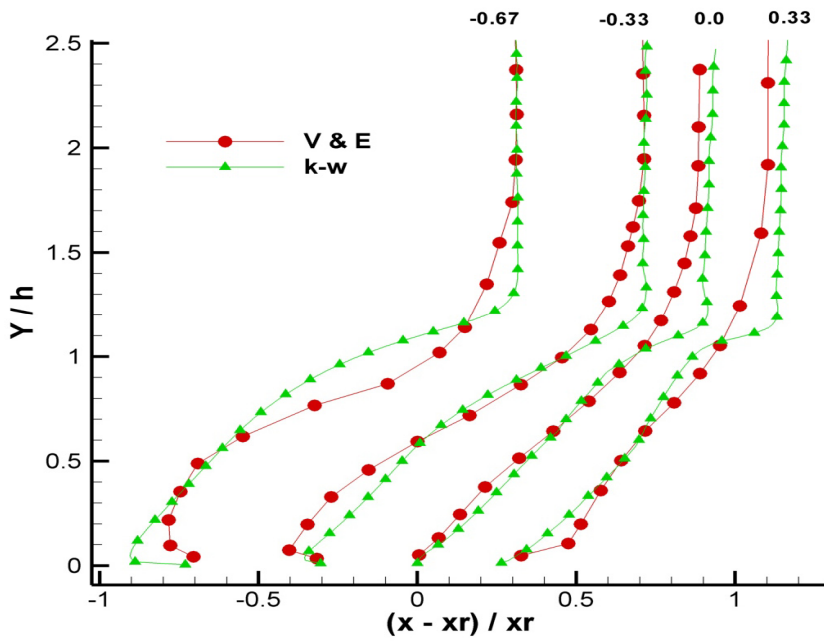


Figure 6: Velocity profiles  $U/U_0$  compared to experimental data (denoted by V&E) for flow behind step at specified locations.

Thermal profile is shown normalized in Fig. 7 as a function of recirculation length and ambient temperature, or inlet temperature and is compared to results from Vogel and Eaton. The distance behind the step is shown as a function of  $x^* = (x-x_r)/x_r$ . The results are in good agreement a short distance above the bottom wall, but the temperature very close to the wall, at the wall node, is too high compared to the data. Also the thermal energy is transported up the step up and circulated back downstream, i.e., thermal energy is advected up the step and then downstream over the top of the recirculation zone. This phenomenon represents the physical process while the flow and thermal transport is developing indicating that the solution hasn't reached steady state at the time depicted here - 1.0623 seconds. The simulated temperature is higher at the wall than measured. This corresponds well with Vogel and Eaton's statement that the maximum temperature rise in the experimental setup with the applied flux is 15 °C above ambient (1985). Also, the comparison near the wall suffers from the aforementioned digitization errors.

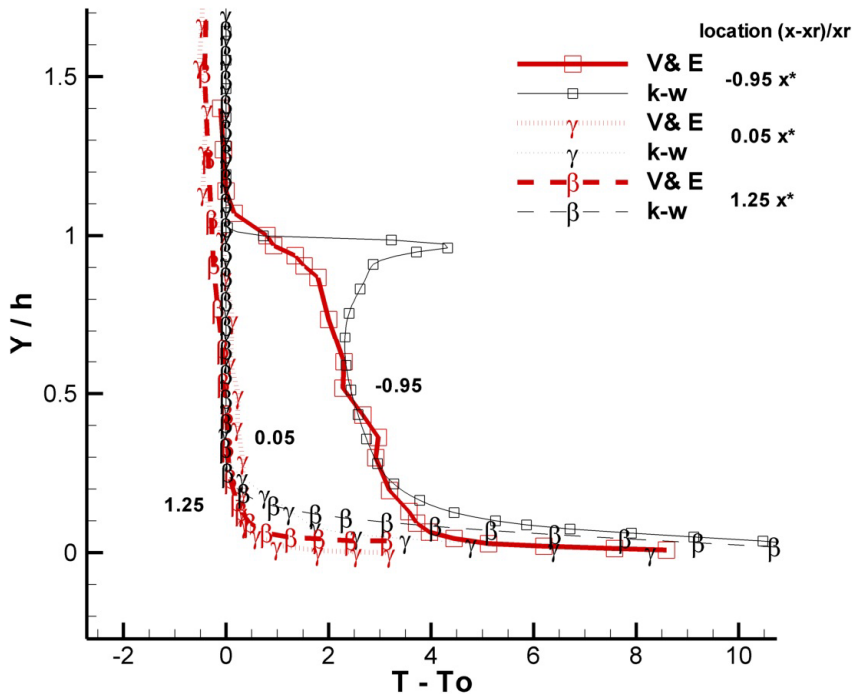


Figure 7: Thermal profiles compared to experiment behind step.

Normalized  $St/\max(St)$  where  $St = q_w/\rho c_p U_o(T_w - T_o)$  number is shown in Fig. 8 as a function of recirculation length and compared to results from Vogel and Eaton. The results compare favorably in the recirculation regime but, the heat flux is shown to be too low downstream of the reattachment location. This suggests that either the solution is not at thermal steady-state after 1.0623 seconds or perhaps a variable turbulent Pr number should be employed as a function of  $y^+$ .

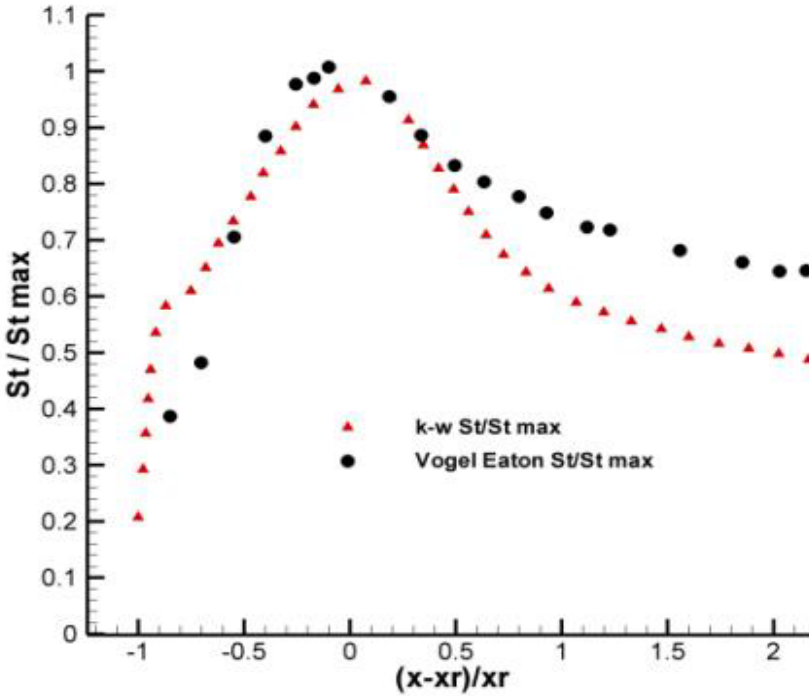


Figure 8: Normalized St number and comparison to experiment behind step.

Table 1 shows results of the recirculation zone length from various researchers. In general the predicted reattachment point has a wide spread, as do the experimental results (Nallasamy, 1987).

## 6 Conclusion

The effective viscosity formulation, as demonstrated with the two-equation closure models in this paper, is reasonably accurate for many engineering type flows, including modeling of combustion, reactive flows, and air pollution in incompressible

Table 1: Recirculation lengths as a function of Re number from various investigators

Re = 47,625	6 6.51 h – $k - w$ FEM Steady State (Ilinca et al., 1998)	Experimental Values $7.0 \pm 0.5$ (Nallasamy M., 1987)
47,625	6.9 h – Algebraic Stress Model (Launder, et al., 1981)	”
47,625	7.2 h – $k - w$ Finite Volume Steady State (Ilegbusi and Spalding, 1983)	“
42,000	7.1 h – 1 <sup>st</sup> -order-in-time $k - w$ FEM (Carrington, 2007 )	“
28,000	6.4 h – 1 <sup>st</sup> -order-in-time low $k - \epsilon$ FEM (Wang, et al., 2009)	6.4 h (Vogel & Eaton, 1985)
This study 28,000	6.4 h – 1 <sup>st</sup> -order-in-time $k - w$ FEM	“

flow regime. The fractional step (projection method) works effectively in conjunction with a locally adaptive grid scheme. Examples using an h-adaptive stabilized (Petrov-Galerkin) finite element framework show the ability to handle complex geometries while minimizing the number of elements required in the model. Element enrichment also works well, while automatically selecting cells for adaptation. The ability to pick regions/cells is useful, although certainly not the most efficient method. The mesh adaptation process will work better with a posterior error method driven by solution from course and finer grids either using a remeshing technique (Pelletier and Ilinca, 1994) or using the enrichment process (Wang and Pepper, 2007).

The boundary layer has good agreement with existing  $k - w$  models and with a DNS formulation for flow in a 2-D duct. The model precisely predicts recirculation for the backward-facing step benchmark. This is a detachment-reattachment problem with adverse pressure gradient. However, the recirculation zone and reattachment lengths are known to be a functions of the arbitrary inlet conditions set for turbulent kinetic energy and dissipation rate and this parameter needs to be set with consid-

eration. Most models do fall short of matching experimental data; the ranges are varying widely as reported by Nallasamy (1987).

The 2<sup>nd</sup> moment methods or algebraic stress models might best be used where the Boussinesq approximation is no longer valid. Turbulence modeling with LES methods is thought to be the direction of the future, but in the near term perhaps some combination of k- $\omega$  and LES is more practical from the point of view of computational requirements.

**Acknowledgement:** Los Alamos National Laboratory, an affirmative action/equal opportunity employer, is operated by the Los Alamos National Security, LLC for the National Nuclear Security Administration of the U.S. Department of Energy under contract DE-AC52-06NA25396. Los Alamos National Laboratory strongly supports academic freedom and a researcher's right to publish; as an institution, however, the Laboratory does not endorse the viewpoint of a publication or guarantee its technical correctness. Reference: LA-UR-09-7843.

## References

**Ainsworth M., Oden, J.T.** (2000): A Posteriori Error Estimation in Finite Element Analysis, John Wiley and Sons, Inc. pp. 20-23.

**Armaly, B.F., Durst, F., Pereira, J.C.F., Schonung, B.** (1983): Experimental and Theoretical Investigation of Backward-Facing Step Flow, *Journal of Fluid Mechanics*, Vol. 127, pp. 473-496.

**Babuska, I.** (1976): The Self-adaptive Approach in the Finite Element Method, The Mathematics of Finite Elements and Applications II: MAFELAP 1975, *Proceedings of the Brunel University Conference on the Institute of Mathematics and Its Applications held in April 1975*, ed. Whiteman, J.R., Academic Press.

**Carrington, D.B., Pepper, D.W.** (2002): Convective Heat Transfer Downstream of a 3-D Backward-Facing Step, *Numerical Heat Transfer, Part A: Applications*, Vol. 41, No. 6-7, pp. 555-578, Taylor and Francis

**Carrington, D. B.** (2007): An h-adaptive k-w Finite Element Model for Turbulent Thermal Flow, Los Alamos National Laboratory, report. LA-UR-06-8432, Los Alamos, NM.

**Chiang T. P., Sheu, T.W.H.** (1999): Time Evolution of Laminar Flow over a Three-Dimensional Backward-Facing Step, *International Journal for Numerical Methods in Fluids*, Vol. 31, pp. 721-745.

**Demkowicz, L., Oden, J.T., Rachowicz, W., Hardy, O.** (1989): Toward a Universal h-p Adaptive Finite Element Strategy, Part 1. Constrained Approximation and

Data Structure, *Computer Methods in Applied Mechanics and Engineering*, Vol. 77, North-Holland, pp. 79-112.

**Gartling, D. K.** (1990): A Test Problem for Outflow Boundary Conditions—Flow over a Backward-Facing Step, *International Journal of Numerical Methods in Fluids*, Vol. 11, pp. 953.

**Heinrich, J. C., Yu, C.-C.** (1988): Finite Elements Simulation of Bouyancy-Driven Flows with Emphasis on Natural Convection in a Horizontal Circular Cylinder, *Computational Methods and Applications in Mechanical Engineering*, Vol. 69, pp. 1-27.

**Hughes J.R.T.** (2000): The Finite Element Method – Linear Static and Dynamic Finite Element Analysis, Dover Publications, Inc., NY.

**Ilegbusi, J. O., Spalding, D. B.** (1983): Turbulent Flow Downstream of a Backward Facing Step, Proc. 4th Int. Symp. on Turbulent Shear Flows, Karlsruhe, West Germany.

**Ilinca, F., Hetu, J.F., Pelletier, D.** (1998): A Unified Finite Element Algorithm for the Two-Equation Models of Turbulence, *Computers & Fluids*, Vol. 27, #3, Elsevier Science, Ltd., pp. 291-310.

**Kelly, D.W., Nakazawa, S., Zienkiewicz, O.C., Heinrich, J.C.** (1980): A Note on Upwinding and Anisotropic Balancing Dissipation in the Finite Element Approximations to Convective Diffusion Problems, *International Journal for Numerical Methods in Engineering*, Vol. 15, John Wiley & Sons, Ltd., pp. 1705-1711.

**Kostas, J., Soria, J., Chong, M.S.** (2002): Particle Image Velocimetry Measurements of a Backward-Facing Step Flow, *Experiments in Fluids*, Vol. 33, pp. 838–853.

**Lacasse, D., Turgeon, E., Pelletier, D.** (2004): On the judicious use of the  $k-\epsilon$  model, wall functions and adaptivity, *International Journal of Thermal Sciences*, Vol. 43, Elsevier Science, Ltd., pp. 925-938.

**Lauder, B.E., Leschziner, M.A., Sinder, M.** (1980-81): Comparison of Computation with Experiment, Summary Report, *AFOSR-HTTM-Stanford Conf. Complex Turbulent Flow: comparison of computation and experiment*, Eds. Kline, S.J., Cantwell, B.J., Lilly, G.M., Stanford University, vol. III, pp. 1390-1407.

**Lin, H., Atluri, S.N.** (2000): Meshless Local Petrov-Galerkin (MLPG) Method for Convection-Diffusion Problems, *CMES: Computer Modeling & Engineering Sciences*, vol.1, no.2, Tech Science Press, pp.45-60.

**Lucas, P., van Zuijlen, A.H., Bijl, H.** (2009): An automated approach for solution based mesh adaptation to enhance numerical accuracy for a given number of grid cells - Applied to steady flow on hexahedral grids, *CMES: Computer Modeling &*

*Engineering Sciences*, vol.41, no.2, Tech Science Press, pp.147-175.

**Naj, H., Mompean, G.** (2009): Computation of the Turbulent Flow in a Square Duct Using a Cubic Low-Reynolds Stress Model, *CMES: Computer Modeling & Engineering Sciences*, vol.53, no.2, Tech Science Press, pp.181-206.

**Nallasmy, M.** (1987): Turbulence Models and Their Applications to the Prediction of Internal Flows: A Review, *Computers and Fluids*, Vol. 15, no. 2, pp. 151-194.

**Pelletier, D., Llinca, F.** (1994): An Adaptive Finite Element Method for Mixed Convection Heat Transfer, AIAA-94-0347, 32<sup>nd</sup> AIAA Aerospace Sciences Meeting.

**Pepper, D.W., Carrington, D.B.** (1997): Convective Heat Transfer over a 3-D Backward-Facing Step, ICHMT International Symposium on Advancements in Computational Heat Transfer, Cesme, Turkey, May 26-30.

**Pepper, D.W., Carrington, D.B.** (1999): Application of h-Adaptation for Environmental Fluid Flow and Species Transport, *International Journal for Numerical Methods in Fluids*, Vol. 32, pp. 275-283, John Wiley & Sons, Inc.

**Pepper, D.W., Carrington, D.B.** (2009): *Indoor Air Pollution Modeling*, Imperial College Press.

**Schlichting, H.** (1979): *Boundary-Layer Theory*, 7<sup>th</sup> edition, McGraw-Hill Inc.

**Schram, C., Rambaud, P., Riethmuller, M.L.** (2004): Wavelet Based Eddy Structure Education from a Backward Facing Step Flow Investigated Using Particle Image Velocimetry, *Experiments in Fluids*, Vol. 36, pp. 233–245.

**Tennekes, H., Lumley, J.L.** (1972): *A First Course in Turbulence*, MIT Press.

**Vertnik, R., Šarler, B.** (2009): Solution of Incompressible Turbulent Flow by a Mesh-Free Method, *CMES: Computer Modeling & Engineering Sciences*, vol.44, no.1, Tech Science Press, pp.65-95.

**Vogel, J.C., Eaton, J.K.** (1985): Combined Heat Transfer and Fluid Dynamic Measurements Downstream of a Backward Facing Step, *Journal of Heat Transfer*, Vol. 107, pp. 922 – 929.

**Wang, X., Pepper, D.W.** (2007): Application of an hp-Adaptive FEM for Solving Thermal Flow Problems, *Journal of Thermophysics and Heat Transfer*, Vol. 21, no.1, pp.190-198.

**Wang, X., Carrington, D.B., Pepper, D.W.** (2009): An Adaptive FEM Model for Unsteady Turbulent Convective Flow Over a Backward-Facing Step, *Journal of Computational Thermal Science*, Begell House Inc., 2009.

**Wilcox, D. C.** (2003): *Turbulence Modeling for CFD*, DCW Industries, La Canada, CA.

**Williams, P. T., Baker, A. J.** (1997): Numerical Simulations of Laminar Flow over a 3D Backward-Facing Step, *International Journal for Numerical Methods in Fluids*, Vol. 24, pp. 1159–1183.

**Zienkiewicz O.C., Zhu, J.Z., Gong, N.G.** (1989): Effective and Practical h-p Version Adaptive Analysis Procedures for the Finite Element Method, *International Journal for Numerical Methods in Engineering*, Vol. 28, John Wiley & Sons, Ltd., pp. 879-891.

**Zienkiewicz O.C., Zhu, J.Z.** 1987): A Simple Error Estimator and Adaptive Procedure for Practical Engineering Analysis, *International Journal for Numerical Methods in Engineering*, Vol. 24, John Wiley & Sons, Ltd., pp. 337-357.